Epidemiol. Infect., Page 1 of 11. © Cambridge University Press 2009
doi:10.1017/S0950268809991178

Understanding influenza virus-specific epidemiological properties by analysis of experimental human infections

C.-M. LIAO[1]*, S.-C. YANG[1], C.-P. CHIO[1] AND S.-C. CHEN[2,3]

[1] *Department of Bioenvironmental Systems Engineering, National Taiwan University, Taipei, Taiwan, ROC*
[2] *Department of Public Health, Chung Shan Medical University, Taichung, Taiwan, ROC*
[3] *Department of Family and Community Medicine, Chung Shan Medical University Hospital, Taichung, Taiwan, ROC*

(*Accepted 23 October 2009*)

SUMMARY

This study aimed to estimate the natural history and transmission parameters based on experimental viral shedding and symptom dynamics in order to understand the key epidemiological factors that characterize influenza (sub)type epidemics. A simple statistical algorithm was developed by combining a well-defined mathematical scheme of epidemiological determinants and experimental human influenza infection. Here we showed that (i) the observed viral shedding dynamics mapped successfully the estimated time-profile of infectiousness and (ii) the profile of asymptomatic probability was obtained based on observed temporal variation of symptom scores. Our derived estimates permitted evaluation of relationships between various model-derived and data-based estimations, allowing evaluation of trends proposed previously but not tested fully. As well as providing insights into the dynamics of viral shedding and symptom scores, a more profound understanding of influenza epidemiological parameters and determinants could enhance the viral kinetic studies of influenza during infection in the respiratory tracts of experimentally infected individuals.

Key words: Epidemiology, infectiousness, influenza, modelling, transmission.

INTRODUCTION

The continuous threat of pandemic human influenza suggests the urgent need for more countries to conduct long-term year-around viral surveillance and to document reliable incidences at (sub)type levels in order to fully understand human influenza, especially in tropical countries where systematic data collection is just starting [1–3]. A parsimonious way of assessing the efficacy of a potential control strategy is to quantify the transmissibility of the infectious virus [4]. Reliable past estimates of transmissibility are rare, especially in (sub)tropical countries. Empirical data documenting infectiousness over time are also limited.

Mathematical models have long been recognized as useful tools in exploring complicated relationships underlying infectious disease transmission processes [4–6]. The accuracy of the predictions obtained from mathematical modelling studies depends on the accuracy of the estimates for the parameters governing the model dynamics. Good parameter estimates are needed to understand and model the potential spread of influenza. Therefore, interpretation of available viral shedding and symptom data from experimental infection studies can provide a platform to link a mathematical model in estimating the efficacies of different measures for influenza infection.

* Author for correspondence: Dr Chung-Min Liao, Department of Bioenvironmental Systems Engineering, National Taiwan University, Taipei, Taiwan 10617 ROC.
(Email: cmliao@ntu.edu.tw)

The dynamics of viral shedding and symptoms following influenza virus infection are key factors when considering epidemic control measures [7–12]. There are three advantages in the experimental influenza virus infection of healthy volunteers that provide a unique opportunity to describe the natural history: (i) the date of infection is known with certainty, (ii) shedding and symptoms are recorded prospectively, and (iii) participants are usually selected with low pre-haemagglutination antibody titres [12].

Although, natural history and transmission parameter estimations take account of only a small portion of the predictability and preparedness in influenza control, they are focal points for epidemiological modelling. Therefore, understanding the mapping relationship between experimental human influenza and infectiousness distribution is needed. Currently, there is no simple mapping relationship between experimental infectious viral load given in terms of 50% tissue culture infective doses ($TCID_{50}$) ml^{-1} of nasal wash and virus-specific infectiousness. Alternatively, the incubation period and transmission data for human influenza can be reanalysed from experimental viral shedding data to derive new natural history parameters, from which a time-profile of infectiousness can be predicted [10, 11].

This predicted infectiousness time-profile can be used to estimate key epidemiological determinants such as basic reproduction number (R_0), disease generation time (T_g), and proportion of transmission occurring prior to symptoms (or asymptomatically) (θ) [13]. R_0 is defined as the expected number of secondary cases generated by the primary case in a wholly susceptible population, whereas T_g is the mean time interval between infection of one person and infection of the person that individual infects [13]. Thus, the epidemiological parameters such as the latent period, the incubation period, and the duration of infectiousness can be estimated.

The aim of the current study was to estimate the natural history and transmission parameters based on experimental viral shedding and symptom dynamics in order to understand the key epidemiological factors that characterize influenza (sub)type epidemics. We present a detailed analysis not only to link experimental viral shedding and symptom data to natural history and transmission parameter estimates but also to relate it to epidemiological parameters. This work can provide clear links between volunteer challenge studies and natural histories and transmission parameterization.

MATERIALS AND METHODS

Experimental viral shedding and symptom data

A valuable dataset provided by Carrat *et al.* [12] provided us with a unique opportunity to examine the linkage between experimental human influenza and natural history parameters. Carrat *et al.* [12] have reviewed the published studies describing the courses of influenza virus infection in placebo-treated and untreated volunteers challenged with wild-type influenza A(H1N1), A(H3N2), and type B. Overall, the data were reconstructed by taking into account 56 different studies with 1280 healthy participants aged between 18 and 40 or 50 years. A total of 532 volunteers were challenged with an A(H1N1) virus, 473 with an A(H3N2) virus, and 189 with a type B virus. The inoculums ranged from 10^3–$10^{7\cdot2}$ $TCID_{50}$ ml^{-1}. Most studies included daily follow-up with daily nasal washing and collection of clinical signs and symptoms.

For all comparisons involving (sub)type influenza viruses, Carrat *et al.* [12] used A(H1N1) as the reference group. Carrat *et al.*'s estimates of the mean duration of viral shedding were: A(H1N1), 4·50 days [95% confidence interval (CI) 3·71–5·28]; A(H3N2), 5·14 days (95% CI 4·48–5·80), and type B, 3·70 days (95% CI 1·73–5·66). The proportion of volunteers who developed clinical illness (any symptoms) after experimental influenza virus infections were estimated to be: A(H1N1), 70·8% (95% CI 50·4–85·2); A(H3N2), 64·5% (95% CI 54·6–73·3); and type B, 57·4% (95% CI 35·2–76·9). The daily viral titres are summarized in Table 1. Table 2 gives the daily total symptom scores.

Methodology

The overall proposed methodology used to map the experimental viral shedding, symptom data and natural history parameters, and to estimate the key epidemiological determinants is illustrated in Figure 1. It can be described briefly as follows.

First, nonlinear models were fitted to the experimental viral shedding data (Table 1) by using the nonlinear regression technique to obtain the optimal fitted models that describe the distributions of viral shedding dynamics. To ensure that the experimental viral titres reflected positive infection response, a cut-off viral titre threshold was set, based on reported mean duration values of viral shedding from Carrat *et al.* [12] (Fig. 1*b*). The cut-off threshold can assist

Table 1. *Results of viral shedding in experimental influenza virus infection according to the virus (sub)types**

	Result for number of days											
	1	1·5	2	2·5	3	3·5	4	5	6	7	8	9
A(H1N1)												
	1·78 (0·22)	n.a.	2·98 (0·22)	n.a.	2·53 (0·25)	n.a.	1·81 (0·25)	1·24 (0·30)	0·71 (0·18)	0·51 (0·10)	0·23 (0·06)	n.a.
A(H3N2)												
	2·31 (0·39)	n.a.	3·17 (0·36)	n.a.	2·96 (0·40)	n.a.	3·13 (0·11)	2·35 (0·25)	2·00 (0·24)	1·28 (0·59)	0·42	0·33
Type B												
	1·82	2·94	2·03	2·26	2·49	2·73	3·18	1·95	1·70	0·46	n.a.	n.a.

n.a., Not available.
Values are mean (±S.E.).
* Data are re-analysed from Carrat *et al.* [12] with units in log ($TCID_{50}$ ml^{-1}) of nasal wash.

Table 2. *Results of total symptom scores in experimental influenza virus infection according to the virus (sub)types**

	Result for number of days							
	1	2	3	4	5	6	7	8
A(H1N1)	0·24	0·69	0·86	0·62	0·41	0·28	0·12	0·04
A(H3N2)	0·34	0·64	0·80	0·69	0·59	0·44	0·33	0·16
Type B	0·08	0·99	0·97	0·87	0·35	0·09	0·01	0

* Data are adopted from Carrat *et al.* [12].

with model interpretation by establishing objective criteria that delineate inoculation and onset of infection. Here the area under the viral shedding *vs.* time curve (AUC) was introduced to measure the strength of viral shedding [7], by which transmissibility can then be estimated appropriately (Fig. 1*b*). The AUC provides a single measure for predicting transmissibility. In the current work, a fitted transmission rate based on the 1918 influenza A(H1N1) epidemic in São Paulo, Brazil ($\beta_{A(H1N1)}$) [14] was used as a reference value to calculate transmission rates of A(H3N2) and type B based on estimated AUC as: $\beta_i = \beta_{A(H1N1)} \times AUC_i/AUC_{A(H1N1)}$ (Fig. 1*c*).

To perform the mapping relationship between viral load and infectiousness time-profiles, the basic reproduction number ($R_{0,i}$) was estimated by the well-known equation [4]: $R_{0,i} = \beta_i/\gamma_i$, where γ is the recovery rate (d^{-1}) determined from the threshold-adjusted viral shedding curve (Fig. 1*b*). A best-fit infectiousness distribution can then be obtained by mapping the viral load data based on

$$R_0 = \int_0^\infty \beta(t)\mathrm{d}t = \text{constant}, \tag{1}$$

where $\beta(t)$ is infectiousness at time t since infection [13]. To improve the mapping performance, the nonlinear regression technique was used to best fit the relationship between infectiousness distribution and viral load data. The coefficient of determination (r^2) was applied to judge the mapping performance.

We estimated the probability that a person has not yet developed symptoms, i.e. asymptomatic probability, and the incubation period (time from infection to start of symptoms) from experimental symptom score data [12]. After the fitted models of infectiousness and asymptomatic probability were determined, a time-distribution profile can be constructed (Fig. 1*f*). Based on the constructed time-distribution curves of infectiousness and asymptomatic probability, two important epidemiological determinants of disease generation time (T_g) and asymptomatic proportion (θ) can be calculated by [13],

$$T_g = \frac{\int_0^\infty t\beta(t)\mathrm{d}t}{\int_0^\infty \beta(t)\mathrm{d}t}, \tag{2}$$

$$\theta \equiv \frac{t_{inc} - t_{lat}}{t_{inf}} = \frac{\int_0^\infty \beta(t)S(t)\mathrm{d}t}{\int_0^\infty \beta(t)\mathrm{d}t}, \tag{3}$$

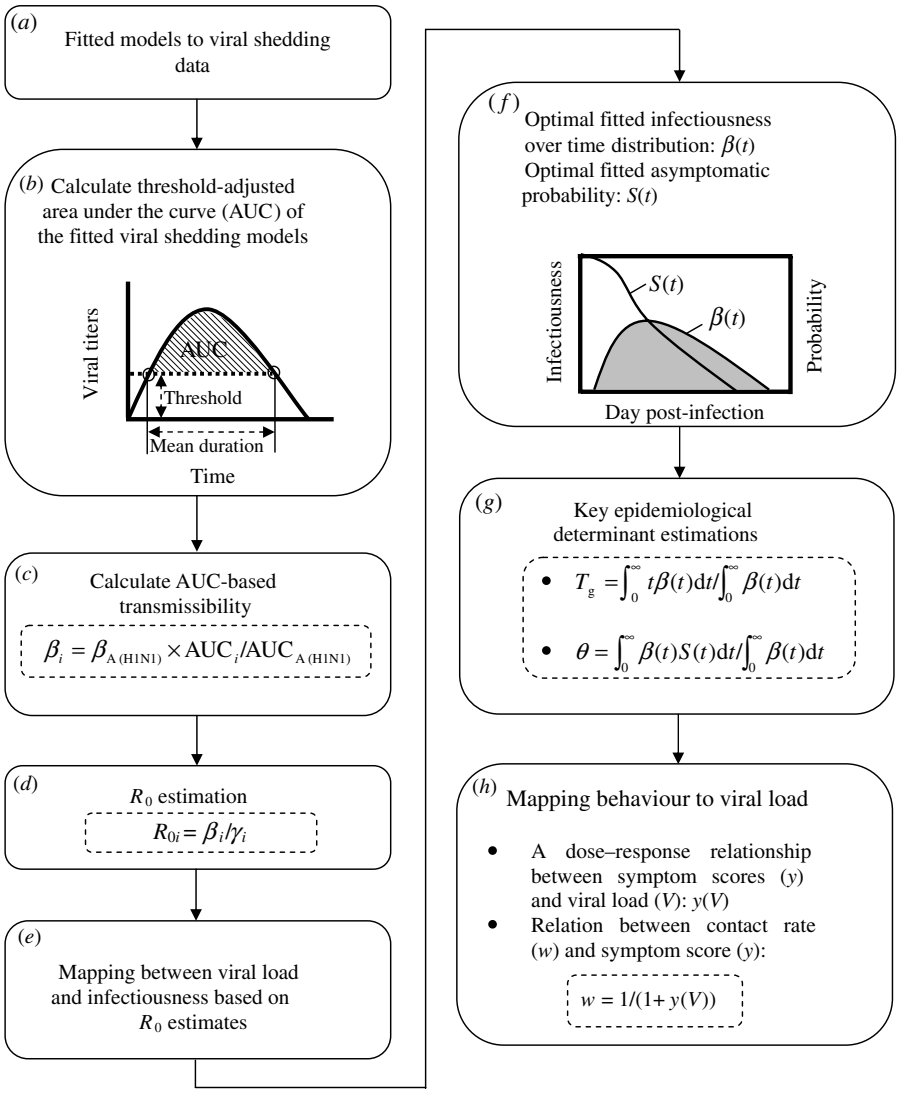

Fig. 1. Flowchart and computational algorithm used in the study (see main text for detailed symbol meanings).

where t_{inc}, t_{lat}, and t_{inf} represent the incubation, latent, and infectious periods, respectively, and $S(t)$ is the asymptomatic probability.

Finally, given the current understanding of the relationships between experimental infections and key epidemiological determinants, we constructed a dose–response relationship between symptom scores and viral load (Fig. 1*h*). The proposed dose–response model can be used to map an individual's contact behaviour to viral load, since contact reduction is dependent on the strength of symptoms [15]. If the symptom score is zero, an infected person feels fine and behaves normally. As symptom scores increase, the contact rate is reduced [15]. Currently, there is no data that capture the influence of contact rate by behavioural changes in symptom scores; therefore, as an alternative, we used a mathematical model [15]:

$$w = \frac{1}{1 + y(V)}, \tag{4}$$

to express the relationship between contact rate (w) and symptom scores (y). The symptom scores (y) can be expressed by the function of viral load (V) by best-fitting a function $y(V)$ to the data from Carrat *et al*. [12].

A Monte Carlo (MC) technique with 10 000 iterations (stability condition) was performed to generate 2·5 and 97·5 percentiles as the 95% confidence intervals for all best-fit models. The MC simulation was implemented using Crystal Ball® software (version 2000.2, Decisionerring Inc., USA). The χ^2 and Kolmogorov–Smirnov (KS) statistics were used to

Table 3. *Optimal fitted equations and probability distribution of viral shedding for influenza virus (sub)types*

Fitted equation*	Probability distribution	r^2
A(H1N1)		
LN4(0·047, 2·91, 2·13, 3·58, 1·82)	LN(1·05, 1·98)†	0·99
A(H3N2)		
LN4(−7·76, 10·98, 2·63, 14·98, 3·71)	LN(1·49, 1·84)	0·98
Type B		
LN4(−703·71, 706·47, 3·04, 1998·50, 214·69)	LN(1·76, 1·57)	0·84

* $\mathrm{LN4}(a,b,c,d,e) = a + b \times \exp\{-\ln 2 \times \ln[1 + (x-c) \times (e^2-1)/(d \times e)]^2/\ln(e)^2\}$.
† LN(GM, GSD) is the lognormal distribution with a geometric mean (GM) and a geometric standard deviation (GSD).

optimize the goodness-of-fit of distribution. All statistical analyses were performed using TableCurve 2D (version 5, AISN Software Inc., USA).

RESULTS

Mapping between viral load and infectiousness

Table 3 summarizes the optimal fitted equations and probability distributions with lognormal function for viral shedding data. Our initial statistical analysis of viral shedding data revealed that the lumped viral shedding threshold (Fig. 2*c*) (i.e. the fixed threshold, was set at 1·6 log $\mathrm{TCID_{50}\,ml^{-1}}$) was more suitable than virus-specific ones (Fig. 2*b*) to derive viral load AUC (Table 4, Fig. 2). Figure 2 shows that A(H3N2) gave the highest viral load AUC (6·09, 95% CI 3·76–8·85) compared to those of type B (3·78, 95% CI 0·11–10·26) and A(H1N1) (2·81, 95% CI 2·41–3·24), leading to the corresponding recovery rates (γ) being estimated as 0·17 $\mathrm{d^{-1}}$ (95% CI 0·15–0·21), 0·20 $\mathrm{d^{-1}}$ (95% CI 0·14–0·68), and 0·30 $\mathrm{d^{-1}}$ (95% CI 0·28–0·32), respectively (Table 4).

Based on the reported reference value of A(H1N1) transmission rate [$\beta_{\mathrm{A(H1N1)}} = 0{\cdot}51\ \mathrm{d^{-1}}$ (95% CI 0·44–0·59)] along with calculated viral load AUC and recovery rates, the resulting estimated average transmission rates were $\beta = 1{\cdot}11\ \mathrm{d^{-1}}$ and $R_0 = 6{\cdot}5$ for A(H3N2), whereas $\beta = 0{\cdot}69\ \mathrm{d^{-1}}$ and $R_0 = 3{\cdot}4$ for type B (Table 4). The results also indicate that the estimated R_0 of A(H1N1) (1·74, 95% CI 1·48–2·04) ranged from 1·7 to 2·0, consistent with the published data [10, 11]. In addition, in order to show the uncertainty of estimated viral-specific transmission rates, we performed MC simulation. The result demonstrates that type B experiences a higher variance than A(H1N1) and A(H3N2) (Fig. 3).

We used the derived R_0 estimates together with experimental viral load data to establish a statistical approach describing the mapping relationship between infectiousness over time and viral load quantitatively. This quantitative statistical analysis demonstrated that the optimal fitted gamma distribution mapped significantly with the viral load data ($r^2 =$ 0·91–0·99) (Table 5, Fig. 4).

Epidemiological determinant and parameter estimation

The disease generation time T_g can be calculated from infectiousness distribution. It resulted in 3·74 days for A(H1N1), 3·79 days for A(H3N2), and 3·57 days for type B [eqn (2), Fig. 4]. The incubation period distribution could be estimated from total symptom-score data in experimental influenza virus infection [12] (Fig. 5*a–c*). Figure 5*a* indicates that the lognormal distributions best describe the model fitting to the data, resulting in a mean incubation period ($\pm$S.D.) of 3·04 $\pm$ 1·28 days for A(H1N1), 3·54 $\pm$ 1·91 days for A(H3N2), and 2·94 $\pm$ 1·50 days for type B.

Once the asymptomatic probability derived from experimental symptom-score data was estimated (Table 5, Fig. 5*d*), the proportion of transmission occurring prior to symptoms θ could be calculated based on eqn (3). The results were $\theta = 0{\cdot}16$ for A(H1N1), 0·18 for A(H3N2), and 0·16 for type B. Finally we estimated the latent periods with the definition of eqn (3) and estimated infectious period ($1/\gamma$) (Table 4). This resulted in a mean latent period estimate of 2·49 days (95% CI 0·71–5·59) for A(H1N1), 2·56 days (95% CI 0·1–7·64) for A(H3N2), and 2·36 days (95% CI 0·38–6·17) for type B. Therefore, the rates at which an exposed individual becomes infectious (i.e. the inverse of the latent period, σ) were

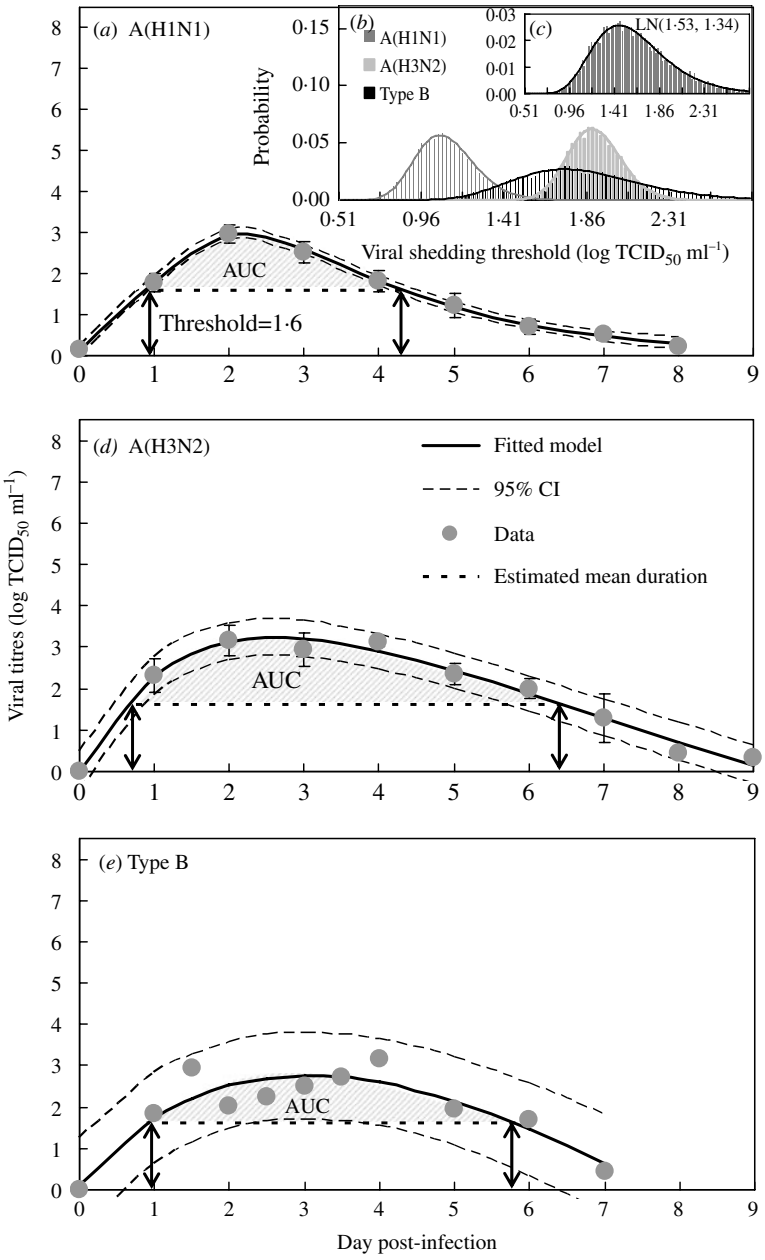

Fig. 2. (*a*) Fitted probability distribution for viral shedding dynamics in experimental influenza A(H1N1) after inoculation. (*b*) Probability distribution of influenza viruses' shedding threshold. (*c*) Probability distribution of lumped viral shedding threshold. (*d*), (*e*) Fitted probability distributions for viral shedding dynamics in experimental influenza A(H3N2) and type B after inoculation, respectively.

calculated as 0·402, 0·391 and 0·424 d^{-1} for A(H1N1), A(H3N2), and type B, respectively.

The optimized logistic regression equation $y=1/(1+(V_0/V)^n)$ best described the dose–response relationship between symptom scores and viral load with fitted parameter values of $V_0=1{\cdot}65$ and $n=1{\cdot}62$ ($r^2=0{\cdot}81$) for A(H1N1); $V_0=2{\cdot}09$ and $n=1{\cdot}61$ ($r^2=0{\cdot}85$) for A(H3N2); and $V_0=1{\cdot}96$ and $n=119{\cdot}08$ ($r^2=0{\cdot}98$) for type B (Fig. 6*a–c*). On the other hand, the normalized contact rate had a functional form of $w=1/(1+(1/(1+(V_0/V)^n)))$ that could be used to reflect the surrogate relationship between contact rate and symptom scores (Fig. 6*d*).

DISCUSSION

Comparison with well-reported data

The experimental human infection-supported statistical approach proposed in this study revealed a

Table 4. *Summary of viral shedding threshold, and threshold adjusted AUC together with recovery rate, transmission rate and basic reproduction number estimates for influenza virus (sub)types*

	Virus (sub)type		
Estimated parameter	A(H1N1)	A(H3N2)	Type B
Viral shedding threshold ($\log \text{TCID}_{50}\ \text{ml}^{-1}$)			
Estimated*	1·08† (0·804–1·439)	1·919 (1·628–2·197)	2·096 (1·236–2·612)
Fixed‡	1·60	1·60	1·60
Threshold adjusted AUC ($\log \text{TCID}_{50}\ \text{ml}^{-1}\ \text{d}$)	2·814 (2·412–3·244)	6·087 (3·755–8·850)	3·778 (0·114–10·262)
Recovery rate, γ (d^{-1})§	0·295 (0·275–0·316)	0·171 (0·146–0·206)	0·203 (0·142–0·677)
AUC-based transmission rate, β (d^{-1})	0·514¶ (0·441–0·593)	1·112‖ (0·686–1·617)	0·690‖ (0·021–1·874)
R_0#	1·742 (1·48–2·04)	6·503 (3·85–9·72)	3·399 (0·06–6·48)

* Estimated based on reported mean duration of viral shedding from Carrat *et al.* [12], as: A(H1N1), 4·50 days (95% CI 3·71–5·28); A(H3N2), 5·14 days (95% CI 4·48–5·80); and type B: 3·70 days (95% CI 1·73–5·66).
† Mean with 95% CI.
‡ Lumped threshold: $1{\cdot}60 \pm 0{\cdot}48$ (mean ± S.D.).
§ Estimated based on Figure 2.
¶ Reference value adopted from Massad *et al.* [14].
‖ $\beta_i = \beta_{A(H1N1)} \times \text{AUC}_i / \text{AUC}_{A(H1N1)}$, where $i = 1, 2$ represent A(H3N2) and type B, respectively.
$R_{0i} = \beta_i / \gamma_i$.

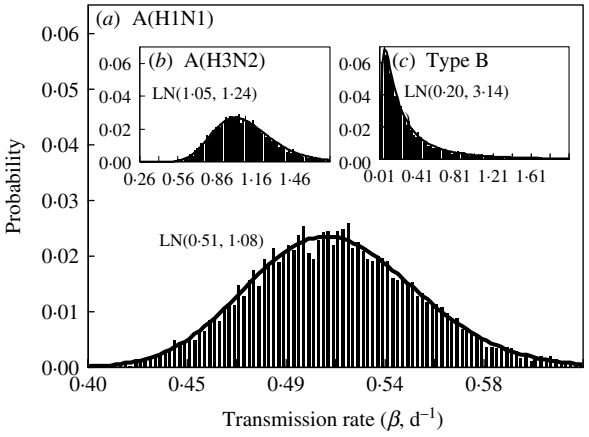

Fig. 3. Probability distributions of transmission rate estimates for influenza (sub)type (*a*) A(H1N1), (*b*) A(H3N2) and (*c*) type B. LN(GM, GSD) denotes the lognormal distribution with geometric mean (GM) and geometric standard deviation (GSD).

Table 5. *Fitted coefficients for infectiousness distribution $\beta(t)$ and asymptomatic probability $S(t)$ of A(H1N1), A(H3N2), and type B (sub)types*

	Fitted coefficients					
Function	*a*	*b*	*c*	*d*	*e*	r^2
A(H1N1)						
$\beta(t)$*	−0·002	0·48	1·99	1·56	1·87	0·99
$S(t)$†	1·004	0·13	−0·32	0·08		0·99
A(H3N2)						
$\beta(t)$	−0·27	1·96	2·89	1·55	3·52	0·96
$S(t)$	0·99	0·11	−0·25	0·06		0·99
Type B						
$\beta(t)$	−3·49	4·33	3·57	0·26	471·73	0·91
$S(t)$	1·03	0·22	−0·43	0·11		0·99

* Gamma distribution is selected as the best-fit model: $f(x) = a + b\ \exp(-(x-c)/d) \times ((((x-c)/d) + e - 1)/(e-1))^{e-1}$.
† Best-fit model: $f(x) = a + bx + cx^{1·5} + dx^2$.

previously undetermined correlation. This correlation links infectiousness over time together with asymptomatic probability profiles and experimental human influenza (sub)type virus infection. Our derived estimates permit evaluation of relationships between various model-derived and data-based estimations, allowing evaluation of trends proposed previously but not tested fully.

A comparison of our derived estimates of key epidemiological parameters with available published data reveals that of the selected reported values of infectious rate for A(H1N1), all have values ranging from 0·50 to 0·53 d^{-1} that agree favourably with our mean estimate of 0·4 d^{-1}. For recovery rate, a mean of 0·3 d^{-1} also fell within the reported range of

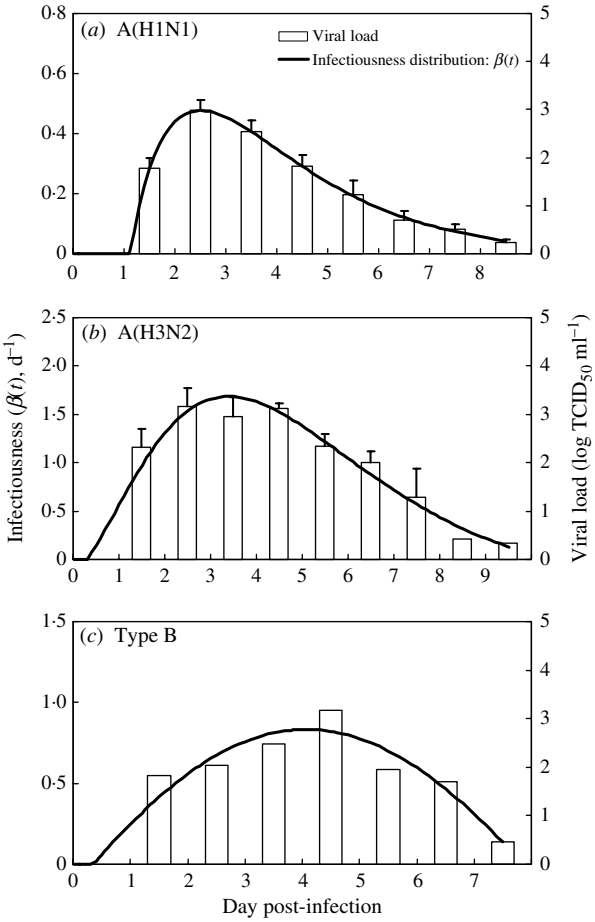

Fig. 4. Mapping between viral load data and fitted infectiousness distribution over time described by the gamma function for influenza (sub)type (*a*) A(H1N1), (*b*) A(H3N2) and (*c*) type B viruses. Error bar represents one standard error from the mean.

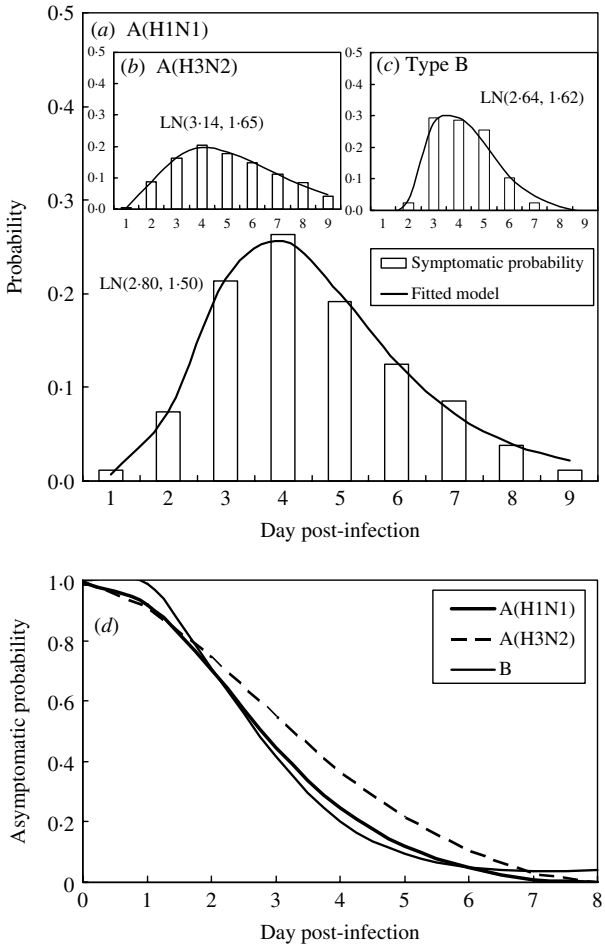

Fig. 5. Fitted models of symptomatic probability for influenza (*a*) A(H1N1), (*b*) A(H3N2) and (*c*) type B viruses. (*d*) Fitted asymptomatic probabilities of three (sub)types viruses. LN(GM, GSD) denotes the lognormal distribution with geometric mean (GM) and geometric standard deviation (GSD).

values of 0·2–0·5 d^{-1} (Table 6). However, it should be noted that our derived R_0 estimate of A(H1N1) (1·74, 95% CI 1·48–2·04) also compared favourably with most reported values with a range of 1·5–4·3 (Table 6).

Of the adopted well-reported parameters of infectious and recovery rates for A(H3N2), only one dataset was available for comparison. It revealed that our infectious rate estimate of 0·39 d^{-1} was slightly less than that of 0·5 d^{-1}, whereas the estimated recovery rate had a mean of 0·17 d^{-1} that agreed significantly with the reported 0·13 d^{-1} (Table 6). However, it is noteworthy that our estimated R_0 of A(H3N2) (6·50) was much greater than those reported values ranging from 1·5–2·5 (Table 6). In fact, we were unable to compare our derived parameters regarding type B owing to lack of available data.

Our data indicated that the latent period was not overlapped the incubation period. We showed that the estimated incubation periods ranged from 3·0 to 3·5 days, whereas it was 2·4–2·6 days for the latent period. Compared with other estimated incubation periods that had a mean value of $1{\cdot}48 \pm 0{\cdot}47$ days based on data from a multiple-exposure event occurring on an aeroplane [10], our estimates appeared to be twice as long as that one. Carrat *et al.* [12] indicated that the most commonly reported incubation periods ranged from 1 to 4 days (average 2 days) deriving from expert opinions or less high-quality evidence. Our result also indicates that the asymptomatic infection (θ) estimates of 16–18% were lower than those of current modelling using ranges of 30–50% [11, 13, 16, 17] and 19–44% [18].

Table 6. *Comparison estimated mean transmission rate (β), infectious rate (σ), recovery rate (γ), and basic reproduction number (R_0) with published literature*

Virus (sub)type	Year	Location	β (d^{-1})	σ (d^{-1})	γ (d^{-1})	R_0	Ref.
A(H1N1)	1978	British	1·66	n.a.	0·46	3·65	[6]
A(H1N1)	1918	Four types of study settings*	n.a.	0·50	0·50	2–4·3	[24]
A(H1N1)	1918	US cities†	n.a.	0·53	0·24	<4	[16]
n.a.	n.a.	n.a.	n.a.	0·33–1·0	0·33–0·5	n.a.	[4]
A(H1N1)	1918	Geneva, Switzerland	8	0·53	0·34	1·49 (1·45–1·53)‡	[25]
			5·75	0·53	0·45	3·75 (3·57–3·93)‡	
A(H1N1)	1918	USA, France, Australia	n.a.	0·53	0·24	1·5–3·0	[26]
A(H3N2)	1968					1·9–2·2	
A(H1N1)	1918	São Paulo, Brazil	0·51	0·07	0·19	2·68	[14]
A(H3N2)						1·5–2·5	
A(H3N2)	1985	France	n.a.	n.a.	0·40	1·5	[27]
A(H3N2)	1968	USSR and Bulgaria	n.a.	0·50	0·13	1·9	[28]
A(H1N1)			0·51§	**0·40**	**0·30**	**1·74**	Current
A(H3N2)			**1·11**	**0·39**	**0·17**	**6·50**	study¶
Type B			**0·69**	**0·42**	**0·20**	**3·40**	

n.a., Not available.

* Confined, communities in Maryland, Scandinavian cities, and cities in the USA.

† US cities including: New York City, Chicago, Philadelphia, Detroit, St Louis, Cleveland, Boston, Baltimore and Pittsburgh.

‡ Mean with 95% CI.

§ Reference value adopted from Massad *et al.* [14].

¶ Estimates obtained from this study are in boldface.

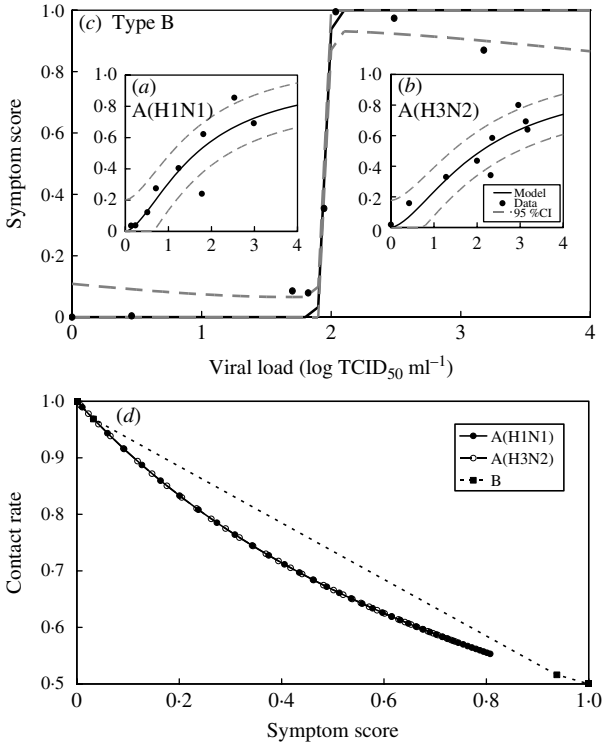

Fig. 6. Relationships between viral loads and normalized symptom scores of influenza (sub)type (*a*) A(H1N1), (*b*) A(H3N2) and (*c*) type B viruses. (*d*) Mapping between symptom scores and contact rate for three (sub)types influenza viruses.

Implication for control measures

Information concerning the dynamics of influenza viral shedding and symptoms during an infection in humans is key for epidemic control strategies [10–13]. They have attracted significant attention because of their intriguing dynamics and their importance in containing influenza epidemics. The precise parameter values of natural history and transmission together with key epidemiological determinants are still not fully determined. Here we analysed the published experimental influenza viral shedding and symptom-score data and evaluated this using well-defined epidemiological representations to characterize the properties that govern population dynamics.

Our statistical analysis with mathematical manipulation demonstrated that we had mapped successfully between viral load and infectiousness over time. This enabled us to estimate natural history parameters such as incubation and latent periods and transmission rate together with key epidemiological determinants of disease generation time, asymptomatic proportion, and basic reproduction number. The proposed dose–response relationship between symptom scores and viral load led to a relation that could map contact rate to viral load [15].

This work could prove to be epidemiologically meaningful and merit further efforts to understand the causes and consequences by placing experimental shedding and symptom data-based natural history and parameters in a predictive framework for complex mitigation strategies in a human influenza pandemic. Beyond offering the confirmation of key epidemiological parameters, our results provide a quantitative metric to assess population dynamics of influenza epidemics using the well-known deterministic SEIR (susceptible, exposed, infectious, recovery) model and improve outcomes [14, 19].

In conclusion, we developed a simple statistical algorithm by combining a well-defined mathematical scheme of epidemiological determinants and experimental human influenza infection. We showed that (i) the observed viral shedding dynamics successfully mapped the estimated time-profile of infectiousness and (ii) the profile of asymptomatic probability was obtained based on observed temporal variation of symptom scores. Besides providing insights into the dynamics of viral shedding and symptom scores, a greater understanding of influenza epidemiological parameters and determinants could enhance viral kinetic studies of influenza during infection in the respiratory tracts of experimentally infected individuals [9, 20]. We also anticipated that direct estimation of natural history and transmission parameters of experimental human influenza, as presented in this study, might provide an important analytical tool to estimate key parameters in experimental and epidemiological studies related to drug-resistant influenza virus in immune response dynamics [15, 21, 22, 23].

DECLARATION OF INTEREST

None.

REFERENCES

1. **Viboud C, *et al.*** Synchrony, waves, and spatial hierarchies in the spread of influenza. *Science* 2006; **312**: 447–451.
2. **Park AW, Glass K.** Dynamic patterns of avian and human influenza in east and southeast Asia. *Lancet Infectious Diseases* 2007; **7**: 543–548.
3. **Finkelman BS, *et al.*** Global patterns in seasonal activity of influenza A/H3N2, A/H1H1, and B from 1997 to 2005: viral coexistence and latitudinal gradients. *PLoS ONE* 2007; **2**: e1296.
4. **Anderson RM, May RM.** *Infectious Diseases of Humans: Dynamics and Control*. UK: Oxford University Press, 1991.
5. **Smith DJ.** Predictability and preparedness in influenza control. *Science* 2006; **312**: 392–394.
6. **Keeling MJ, Rohani P.** *Modeling Infectious Diseases in Humans and Animals*. NJ: Princeton University Press, 2008.
7. **Hayden FG, *et al.*** Safety and efficacy of the neuraminidase inhibitor GG167 in experimental human influenza. *Journal of the American Medical Association* 1996; **275**: 295–299.
8. **Hayden FG, *et al.*** Local and systemic cytokine responses during experimental human influenza A virus infection. *Journal of Clinical Investigation* 1998; **101**: 643–649.
9. **Baccam P, *et al.*** Kinetics of influenza A virus infection in humans. *Journal of Virology* 2006; **80**: 7590–7599.
10. **Ferguson NM, *et al.*** Strategies for containing an emerging influenza pandemic in Southeast Asia. *Nature* 2005; **437**: 209–214.
11. **Ferguson NM, *et al.*** Strategies for mitigating an influenza pandemic. *Nature* 2006; **442**: 448–452.
12. **Carrat F, *et al.*** Time lines of infection and disease in human influenza: a review of volunteer challenge studies. *American Journal of Epidemiology* 2008; **167**: 775–785.
13. **Fraser C, *et al.*** Factors that make an infectious disease outbreak controllable. *Proceedings of the National Academy of Sciences USA* 2004; **101**: 6146–6151.
14. **Massad E, *et al.*** The 1918 influenza A epidemic in the city of São Paulo, Brazil. *Medical Hypotheses* 2007; **68**: 442–445.
15. **Handel A, Longini Jr. IM, Antia R.** Neuraminidase Inhibitor resistance in influenza: assessing the danger of its generation and spread. *PLoS Computational Biology* 2007; **3**: 2356–2464.
16. **Mills CE, Robins JM, Lipsitch M.** Transmissibility of 1918 pandemic influenza. *Nature* 2004; **432**: 904–906.
17. **Germann TC, *et al.*** Mitigation strategies for pandemic influenza in the United States. *Proceedings of the National Academy of USA* 2006; **103**: 5935–5940.
18. **Liao CM, Chen SC, Chang CF.** Modelling respiratory infection control measure effects. *Epidemiology and Infection* 2008; **136**: 299–308.
19. **Liao CM, Chen SC.** Modelling control measures to reduce the impact of pandemic influenza among schoolchildren. *Epidemiology and Infection* 2008; **136**: 1035–1045.
20. **Larson EW, *et al.*** Influenza virus population dynamics in the respiratory tract of experimentally infected mice. *Infection and Immunity* 1976; **13**: 438–447.
21. **Stilianakis NI, Perelson AS, Hayden FG.** Emergence of drug resistance during an influenza epidemic: insights from a mathematical model. *Journal of Infectious Diseases* 1998; **177**: 863–873.
22. **Ferguson NM, *et al.*** A population-dynamic model for evaluating the potential spread of drug-resistant influenza virus infections during community-based use of

antivirals. *Journal of Antimicrobial Chemotherapy* 2003; **51**: 977–990.

23. **Regoes RR, Bonhoeffer S.** Emergence of drug-resistant influenza virus: Population dynamical considerations. *Science* 2006; **312**: 389–391.
24. **Vynnycky E, Trindall A, Mangtani P.** Estimates of the reproduction numbers of Spanish influenza using morbidity data. *International Journal of Epidemiology* 2007; **36**: 881–889.
25. **Chowell G, *et al.*** Transmission dynamics of the great influenza pandemic of 1918 in Geneva, Switzerland: assessing the effects of hypothetical interventions. *Journal of Theoretical Biology* 2006; **241**: 193–204.
26. **Chowell G, Miller MA, Viboud C.** Seasonal influenza in the United States, France, and Australia: transmission and prospects for control. *Epidemiology and Infection* 2008; **136**: 852–864.
27. **Flahault A, *et al.*** Modelling the 1985 influenza epidemic in France. *Statistics in Medicine* 1988; **7**: 1147–1155.
28. **Rvachev LA, Longini Jr. IM.** A mathematical model for the global spread of influenza. *Mathematical Biosciences* 1985; **75**: 3–22.